

Geometry-induced fluctuations in the transitionally rough regime

Nabil Abderrahaman-Elena

Department of Engineering
University of Cambridge
Trumpington Street. CB2 1PZ. UK
na409@cam.ac.uk

Ricardo García-Mayoral

Department of Engineering
University of Cambridge
Trumpington Street. CB2 1PZ. UK
r.gmayoral@eng.cam.ac.uk

ABSTRACT

Direct numerical simulations of turbulent flows over rough surfaces are conducted to investigate the physics of the transitionally rough regime. Different roughness sizes are analysed within the transitional regime, for a given roughness shape. We decompose the flow into a turbulent, geometry-independent contribution, and a geometry-induced contribution, whose intensity is modulated by the overlying turbulence. In the onset of the transitionally rough regime, the turbulent component remains essentially unmodified compared to smooth-wall turbulence, and the roughness effects can be attributed entirely to the geometry-induced fluctuations. As the roughness size increases further, the turbulent component is also modified, and the effect of the surface on the flow becomes more complex.

INTRODUCTION

In industrial applications, roughness usually has an undesirable impact as it generates additional mixing near the wall, which results in an increase of drag. In other applications, however, this additional mixing can be beneficial, for instance enhancing heat transfer. Research on rough-wall turbulence is vast and dates back to Darcy (1857). Extensive reviews of the subject can be found in Raupach *et al.* (1991), Jiménez (2004) and Flack & Schultz (2010). For turbulent flows, provided that the characteristic size of roughness is still too small to affect the flow, rough surfaces behave as smooth walls, in what is known as the hydraulically smooth regime. However, for a fixed roughness of characteristic size k , as the Reynolds number increases the value of k^+ increases, where the superscript '+' denotes scaling in wall-units. For a sufficiently large Reynolds number, the roughness begins to affect the turbulent flow as k^+ is no longer negligible. Eventually, k^+ becomes large enough for inertial terms to dominate even in the roughness sublayer, which is the region in which turbulent fluctuations depend predominantly on the roughness geometry (Schultz & Flack, 2007). The pressure drag then dominates and the friction becomes independent of viscosity. The friction coefficient reaches an asymptotic state in which it becomes independent of the Reynolds number. This is known as the fully rough turbulent regime. For values of k^+ between the hydraulically smooth and the fully rough regimes, the flow is said to be transitionally rough. This is the regime considered in this work.

Because of the complexity of any real rough geometry, it is desirable to find a simple way to characterise roughness. Nikuradse (1933) conducted a series of experiments in pipe flows where the walls were coated with packed sand grains of equal size, with measurements taken for several sand grain sizes. The parameter chosen to characterise the different cases was the sand grain mean diameter, k_s . Hama (1954) found that far from the wall roughness only modifies the mean velocity profile by a shift ΔU^+ . In the logarithmic region, the shape of the profile and Kármán constant, κ , are otherwise unaffected,

$$U^+(y^+) = \kappa^{-1} \log y^+ + 5.1 - \Delta U^+. \quad (1)$$

Schlichting (1936) found that k_s^+ could be used to characterise any flow over roughness. The strategy is then not to consider the actual roughness size, k^+ , but instead to find the equivalent sand grain roughness, k_s^+ , which gives the same ΔU^+ as the actual roughness. Any flow with an equivalent sand roughness of k_s^+ produces the same ΔU^+ as a sand roughness of grain size k_s^+ . In the fully rough regime, k_s^+/k^+ becomes constant and is only a function of the geometry. However, in the transitionally rough regime k_s^+/k^+ is variable and depends on the flow also. An alternative parameter is $k_{s_{\infty}}^+$, which is equal to k_s^+ in the fully rough regime, but maintains a constant ratio $k_{s_{\infty}}^+/k^+$ even in the transitional regime (Jiménez, 2004). As a result, the ratio $k_{s_{\infty}}^+/k^+$ depends only on the geometry in all the regimes, but different geometries exhibit a different ΔU^+ for the same $k_{s_{\infty}}^+$ in the transitional regime, as illustrated in figure 2(a). Still, ΔU^+ curves eventually collapse in the fully rough regime.

Starting from $k^+ \approx 0$, as k^+ increases and roughness begins to affect the viscous sublayer, friction deviates from hydraulically smooth values, and the flow enters the transitionally rough regime. Some experimental works pay special attention to this regime (Flack *et al.*, 2012; Flack & Schultz, 2014). However, one of the key questions remains unresolved: what mechanism triggers the departure from the hydraulically smooth regime as k^+ increases; and how to define a threshold for this transition based on the roughness geometry only. One of the main issues is that, while $k_{s_{\infty}}^+$ characterises appropriately the fully rough regime for most rough surfaces, it appears to not be the correct parameter in the transitionally rough regime. This was already noticed by Colebrook (1939) as his results and Nikuradse's do not match in the mentioned transitional regime. In general, different geometries of roughness lead to different transitions. Comparing several sizes and combinations of sand grains, Colebrook & White (1937) proposed this transition is abrupt in organised geometries, while the presence of a wider range of roughness sizes makes the transition smoother. This assumption is also supported by more recent experiments, such as those using uniformly arranged spherical rough elements by Ligrani & Moffat (1986), in which the transition takes place not only for even higher values of $k_{s_{\infty}}^+$, compared to Nikuradse's and Colebrook's experiments, but also in a sharper manner. Moreover, the discrepancy is such that Flack & Schultz (2010) report a relatively wide range of experimental values in which the transition takes place, spanning between $1.4-15 < k_s^+ < 18-70$.

Recent research by Chung *et al.* (2015) is aiming to find a methodology to capture the effect of roughness, particularly the increase in friction and ΔU^+ , at a minimum cost. They conduct fully turbulent simulations, but in minimal-span boxes (Jiménez & Moin, 1991; Flores & Jiménez, 2010) that reduce the computational requirements. The present project also aims to eventually provide estimates for ΔU^+ at a reduced cost, but removing the need to carry out turbulent simulations altogether, by capturing the effect of the geometry with reduced order models.

To produce such models, we aim to gain insight into the physics triggering the transition from the hydraulically smooth

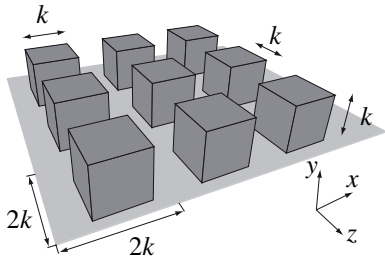


Figure 1. Sketch of the roughness geometry over the bottom wall.

regime. We carry out a series of direct numerical simulations (DNSs) of turbulent channels with rough walls. We study a roughness texture formed by equispaced square posts of side k in a rectangular arrangement and a texture period $s = 2k$, as sketched in figure 1. Similar geometries have been studied by other authors (Leonardi *et al.*, 2007; Leonardi & Castro, 2010) although their simulations mainly explore the fully rough regime. The purpose of our simulations is to investigate the evolution of turbulent flow fluctuations through the transitionally rough regime. The surface shape is kept constant throughout the simulations, but the size of the elements measured in wall units is varied from $k^+ \approx 6$ to $k^+ \approx 38$, aiming to span the whole regime. The parameters for the simulations are summarised in table 1. We aim to decompose the fluctuation into turbulent and roughness-induced contributions, with the purpose of isolating the effect of the roughness geometry.

The numerical experiments are conducted in a turbulent periodic channel with rough texture on the top and bottom walls. The streamwise, wall-normal and spanwise coordinates are x , y and z , with u , v and w the corresponding components of the velocity. The numerical method is described in Abderrahaman-Elena & García-Mayoral (2016). The channel half-height, δ , is measured from the roughness tips, the length is $L_x = 2\pi\delta$ and the width $L_z = \pi\delta$. In order to solve the flow around the roughness elements, the grid resolution is increased near and within the roughness region, $\Delta_{x_w}^+ = \Delta_{z_w}^+ \approx 1-2$, and $\Delta y_{min}^+ \approx 0.31$.

The friction Reynolds, $Re_\tau \approx 185$, is computed using δ and the friction velocity u_τ obtained by extrapolating the total shear to an effective channel height δ' . This height is set so that $u_\tau^2 = -\delta' \partial p / \partial x$ (García-Mayoral & Jiménez, 2011b; Chung *et al.*, 2015), which is the relationship that would hold for a smooth channel at δ . The virtual origin calculated from the DNS and the Stokes approximation are shown in figure 2(c).

GEOMETRY-INDUCED FLUCTUATIONS

In the range of k^+ studied, our geometry displays conventional k -roughness behaviour (Jiménez, 2004), i.e. friction increases with k^+ and the mean velocity profile is shifted downwards, as shown in figure 2(b), increasing drag. In order to quantify this shift on the velocity profile and also be able to establish a comparison with other surfaces, we have included in figure 2(a) the results for the roughness function, ΔU^+ , versus $k_{s_{\infty}}^+$ for the geometry considered, which satisfies $k_{s_{\infty}}/k \approx 0.5$. As $k_{s_{\infty}}^+$ collapses the fully rough regime to a single asymptote, the variations in the transitional regime for different surfaces can be compared. The roughness function of our cases is also compared to the results of Colebrook & White (1937), Nikuradse (1933), and Ligrani & Moffat (1986). In Colebrook & White (1937), Colebrook (1939), and Nikuradse (1933) the transition is smooth and begins at low values of $k_{s_{\infty}}^+$. In our case, the transitional regime resembles more closely that of the packed spheres of Ligrani & Moffat (1986), evolving rapidly from low to high values of ΔU^+ . This is in agreement with the observation by Colebrook (1939) that regular roughness departs from the hydraulically smooth regime more gradually than regular roughness.

Table 1. Parameters of the simulations. s^+ is the post spacing in both the streamwise and spanwise directions. The number of collocation points in the fine grid near the roughness are N_{x_w} and N_{z_w} along the streamwise and spanwise directions respectively.

Case	k^+	s^+	ΔU^+	Re_τ	N_{x_w}	N_{z_w}
0C	—	—	—	184.5	192	192
6C	6.1	12.1	0.63	184.9	1152	576
9C	9.0	18.0	1.07	183.1	768	384
12C	12.0	24.0	1.90	183.6	1152	576
18C	17.8	35.5	3.81	181.0	768	384
24C	23.5	47.0	5.29	179.4	576	288
36C	37.9	75.8	7.37	193.0	768	384

To understand how the flow is modified by the presence of roughness and produces the changes described above, we focus our analysis on the velocity fluctuations. The effect of roughness is limited to the vicinity of the wall, and decays rapidly away from it. Figure 3 portrays an instantaneous realization of the streamwise velocity for case 9C at $y^+ \approx 1.3$ above the roughness peaks, close enough to the wall to observe the effect of the roughness elements. The figure shows that the fluctuating velocity signal has two distinct contributions. The first is the typical background signal characteristic of smooth-wall turbulence, which consists of streamwise elongated streaks of high and low u -velocity, of length 500 – 1000 wall units and width 50 – 100 wall units (Kim *et al.*, 1971; Smith & Metzler, 1983). This contribution remains essentially unmodified, at least for $k^+ < 15$ (or $\Delta U^+ < 3$). The second contribution is directly caused by the presence of the roughness elements, and consists of alternating regions of relatively low velocity right over the protruding elements, and relatively high velocities over the valleys between elements. This signal is attached to the roughness geometry, and is therefore not advected in time as the turbulent contribution. It is instead essentially repeated periodically in a lattice of streamwise and spanwise periodicity s , so that its value depends only on the relative position within each periodic unit, that is, the coordinates \tilde{x} and \tilde{z} , with values between 0 and s , and the wall normal coordinate y . The lengthscales of this roughness contribution would scale with k^+ , and its intensity would also increase with the roughness size.

To characterise these two contributions, a typical decomposition is

$$\mathbf{u}(x, y, z, t) = \mathbf{U}(y) + \mathbf{u}'_T(x, y, z, t) + \bar{\mathbf{u}}_R(\tilde{x}, y, \tilde{z}), \quad (2)$$

where $\bar{\mathbf{u}}_R$ is the spatially fluctuating, time-independent component due to the roughness, and \mathbf{u}'_T the remaining turbulent signal, which includes the mean velocity $\mathbf{U}(y)$ and the fluctuating component \mathbf{u}'_T . The geometry-coherent signal $\bar{\mathbf{u}}_R$ can be obtained by averaging over time and over the roughness lattice,

$$\bar{\mathbf{u}}_R(\tilde{x}, y, \tilde{z}) = \langle \mathbf{u}(x, y, z, t) - \mathbf{U}(y) \rangle_{t, N_R}, \quad (3)$$

where N_R is the number of roughness elements in the simulation domain.

The above decomposition is analogous to that of Reynolds & Hussain (1972) for coherent waves in turbulence, and is widely used in flows over complex surfaces (Choi *et al.*, 1993; Jiménez *et al.*,

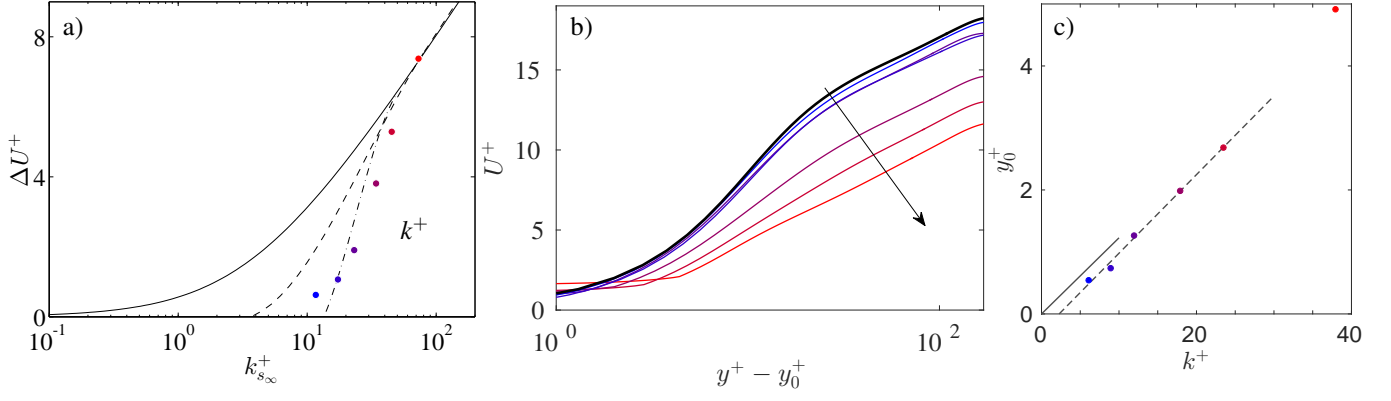


Figure 2. (a) Roughness function ΔU^+ ; —, correlation for Colebrook results (Jiménez, 2004); ----, correlation of sand grain roughness (Nikuradse, 1933); - · -, correlation of sphere roughness (Ligrani & Moffat, 1986); ● present DNSs.. (b) Mean velocity profiles measured from $y_0^+ = 1/8 k^+$. Thick black line, case 0C. (c) Protrusion height, y_0^+ . Solid line, solution of Stokes problem, with the slope $dy_0^+/dk^+ \approx 1/8$. Dashed line, linear regression for cases 6C to 24C. Blue to red cases 6C through 36C of table 1

2001; García-Mayoral & Jiménez, 2011b; Jelly *et al.*, 2014; Seo *et al.*, 2015). However, this decomposition fails to completely separate the two contributions, since when \bar{u}_R is subtracted from u , u_T still carries the signature of roughness. The problem is illustrated in figure 3, which portrays the different components at a given instant and $y \approx 1.3$ above the roughness crest, for case 9C. For this case k^+ is still small enough for the rough and turbulent components to have clearly separate wavelengths, so that u_T can be obtained simply by filtering out small wavelengths. Panels 3(a) and (b) show the full velocity signal u and the filtered turbulent contribution u_T , and illustrate the starting hypothesis that the velocity signal is made up of a turbulent signal, analogous to that over smooth walls, plus a small-intensity, small-wavelength, roughness-coherent signal. However, when u_T is subtracted from u , as shown in panel 3(d), the result is not \bar{u}_R , as in figure 3(c). However, the subtraction resembles closely the modulation in amplitude of \bar{u}_R by the turbulent contribution u_T .

$$u_R = \frac{u_T}{U} \bar{u}_R. \quad (4)$$

Note that, on average, u_T/U is equal to 1.

Taking the above discussion into account and expanding it to the other velocity components, we propose the following decomposition

$$u = u_T + u_R = u_T + \frac{u_T}{U} \bar{u}_R + \frac{w_T}{U} \bar{u}_{R\perp}, \quad (5)$$

$$v = v_T + v_R = v_T + \frac{u_T}{U} \bar{v}_R + \frac{w_T}{U} \bar{v}_{R\perp}, \quad (6)$$

$$w = w_T + w_R = w_T + \frac{u_T}{U} \bar{w}_R + \frac{w_T}{U} \bar{w}_{R\perp}. \quad (7)$$

The second term on the right-hand-side captures the effect of the flow around the roughness elements, driven by the local streamwise turbulent contribution u_T . Similarly, the last term on the right-hand-side, the one including the subscript ‘ \perp ’, accounts for the flow around the roughness elements when driven by the local spanwise turbulent contribution w_T .

For large k^+ , the length-scales of the turbulent and the roughness-induced components become comparable, and the two contributions cannot then be simply separated filtering out the roughness component. However, it is always possible to obtain $\bar{\mathbf{u}}_R$ from equation (3) and the turbulent contributions can then be obtained algebraically from equations (5)-(7). As an example, figure 4 shows the agreement between $u - u_T$ and u_R , $v - v_T$ and v_R ,

and $w - w_T$ and w_R , where the T -subscript magnitudes have been obtained by filtering out the small scales and the R -subscript magnitudes have been obtained algebraically. The comparisons on the bottom panels show how neglecting the amplitude modulation of u_R could lead to underpredicting its contribution to the total intensity of the fluctuations.

The present modulation of the near-wall, roughness-induced flow by the overlying turbulent flow is similar to the modulation of buffer-layer turbulence by outer-layer large structures (Mathis *et al.*, 2009; Talluru *et al.*, 2014; Zhang & Chernyshenko, 2016), except for the difference in the scales involved and the lack of modulation in wavelength. In the present study, the modulating signal is actually the buffer-layer turbulence. The low Reynolds number of our DNSs prevents the development of large-scale turbulence, but if this was present it could be expected to modulate the buffer-layer flow. In turn, the total turbulent velocity above each roughness element would modulate the local u_R .

The modulation of u_R by the overlying turbulence is also connected to the concept of protrusion height in riblets (Luchini *et al.*, 1991; García-Mayoral & Jiménez, 2011a). For vanishing riblet spacing, the flow near each texture element is produced by the quasi-uniform shear induced by the turbulent eddy just above. In the scale of the texture, this eddy can be represented as quasi-homogeneous and quasi-steady (Zhang & Chernyshenko, 2016). The overlying turbulent velocity therefore sets the scale for the local velocity within the riblet grooves, just like in our case the overlying u_T sets the scale for the local u_R .

In the limit of vanishingly small texture, the roughness-induced component is essentially the result of a quasi-homogeneous, quasi-steady flow. We explore this idea in order to predict this contribution without carrying out full DNSs. We find that $\bar{\mathbf{u}}_R$ is not accurately represented by the Stokes solution, not even for the smallest roughness size. However, the solution obtained for a shear-driven, laminar simulation matching k^+ seems to display a fairly good agreement with the roughness-induced contribution, even well beyond the sizes by which we would expect it to start failing, as it appears to be a good approximation at least up to $k^+ \approx 18$, as shown in figure 5.

The above discussion is only valid for vanishingly small roughness, when u_T modulates u_R but is itself unaffected by the presence of roughness. However, as the roughness size increases and becomes comparable to the turbulent eddies, this assumption ceases to hold. For the geometry considered in this paper, we would expect this to happen for $s^+ \approx 15 - 20$, when the spacing between rough-

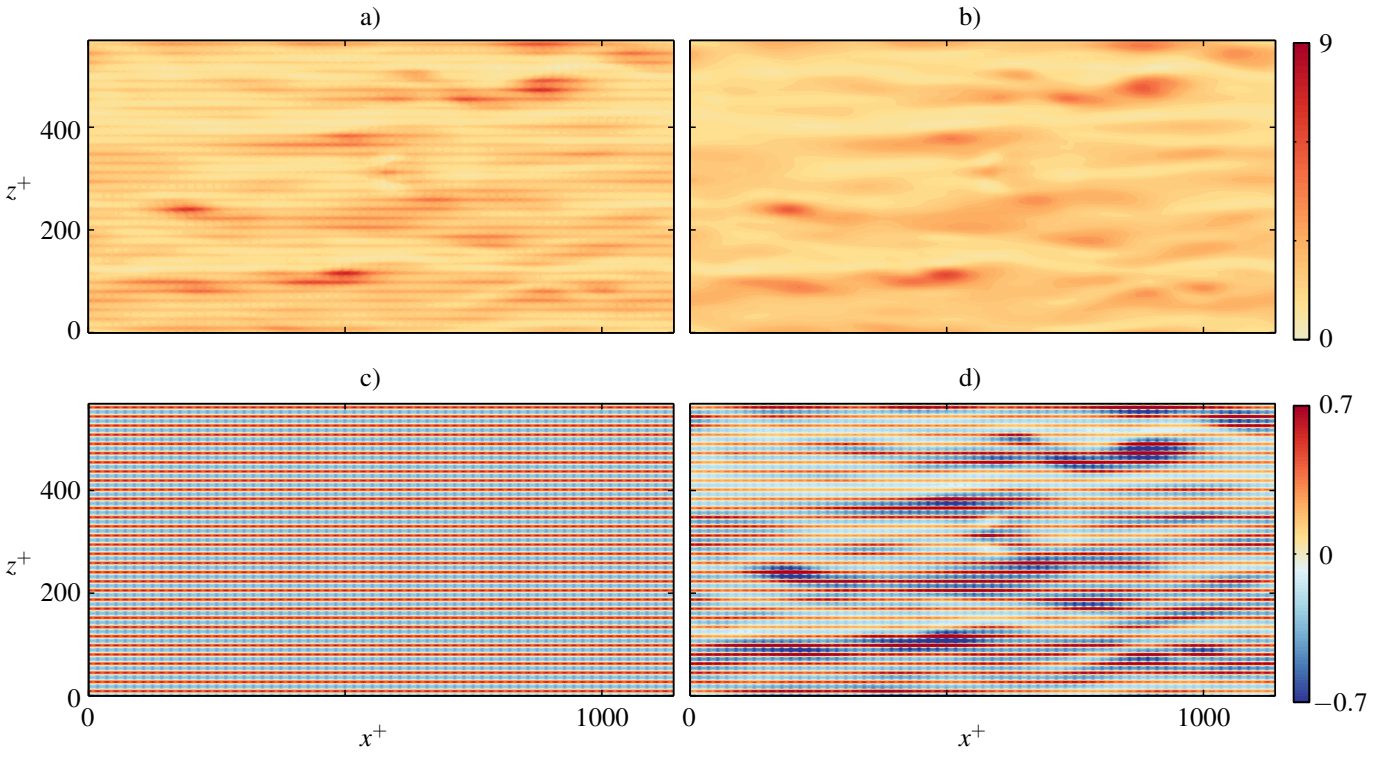


Figure 3. Instantaneous components of the streamwise velocity at $y^+ \approx 1.3$ above roughness crest for case 9C. (a) Full velocity signal u . (b) Background turbulent contribution u_T . (c) Coherent, time average signal induced by the presence of roughness, \bar{u}_R . (d) Instantaneous $u - u_T$; u_T -modulated signal induced by the roughness, u_R .

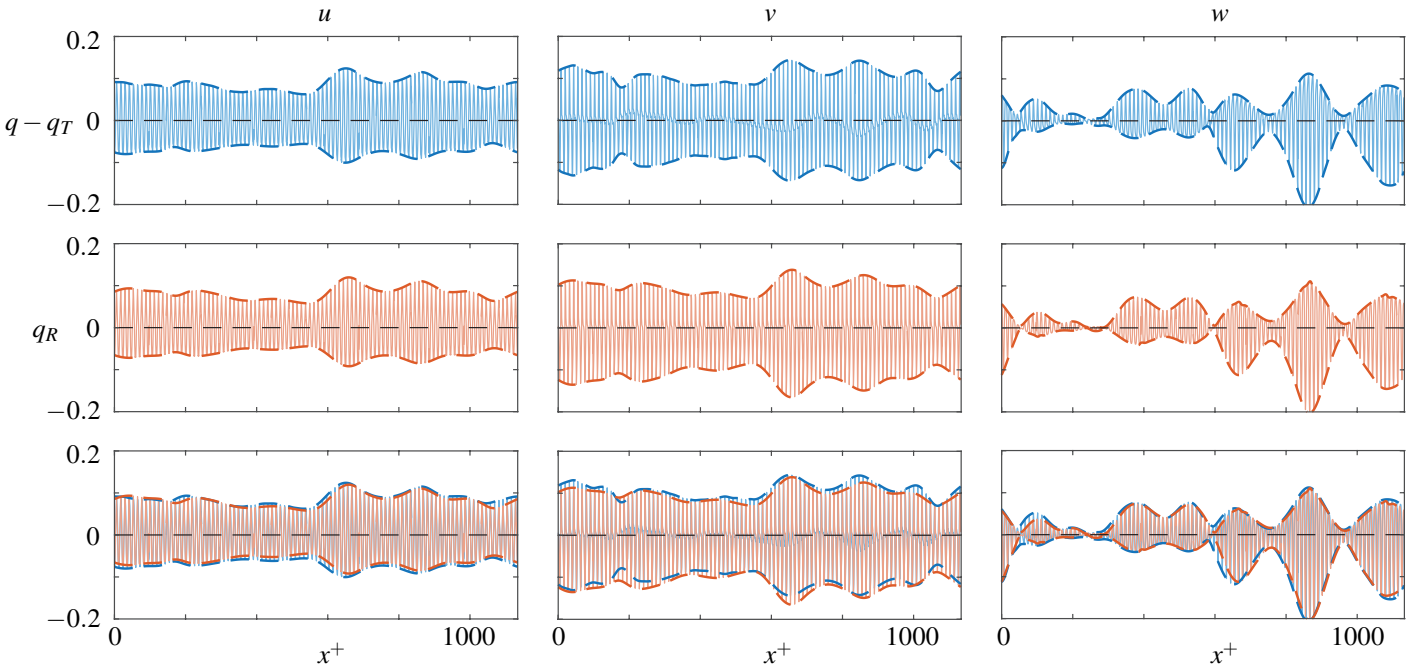


Figure 4. Instantaneous components of the streamwise velocity for case 6C at $y^+ \approx 0.7$ above roughness crest. In solid blue, total velocity signal minus its turbulent contribution. In solid red, modulated roughness-induced fluctuation. Dashed lines indicate the envelope. The variable q represents either u , v or w .

ness elements becomes comparable to the typical diameter of the quasi-streamwise vortices that are characteristic of near-wall turbulence (Kim *et al.*, 1987). The validity of the assumption that the turbulent contribution remains essentially unaffected by the presence of roughness can be checked in figure 6, which compiles the

rms of the different contributions of $\langle u' \rangle$, $\langle v' \rangle$ and $\langle w' \rangle$, as a function of y^+ . In figure 6, the two rightmost columns of panels show how the phase-averaged and the modulated roughness-induced contributions increase gradually with k^+ from the smallest roughness, while significant changes in the turbulent components only appear

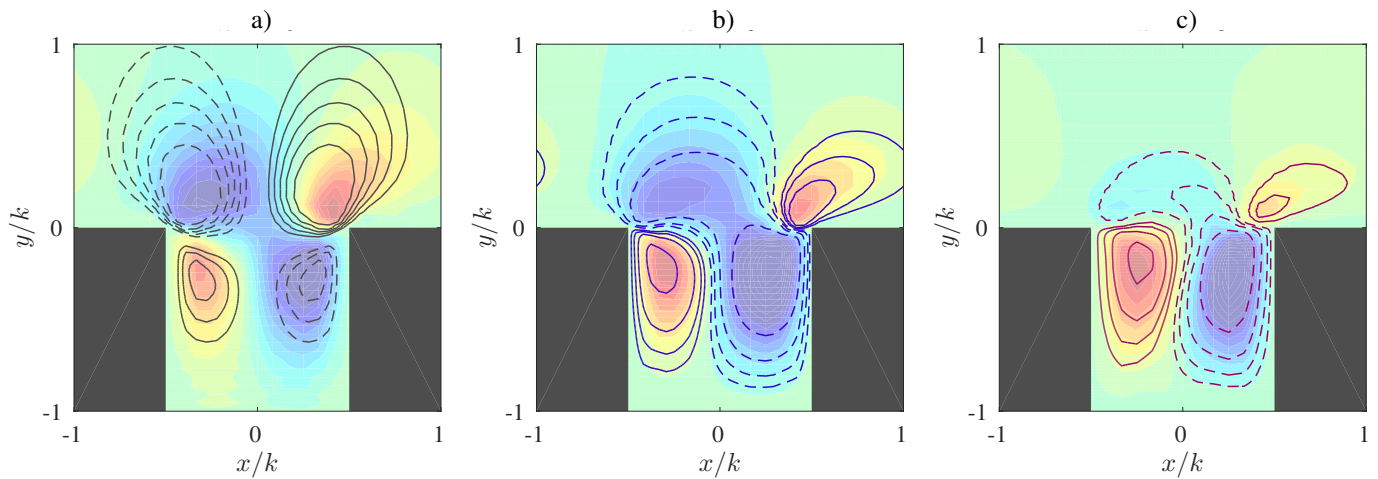


Figure 5. Wall-normal velocity in an x - y cross-section halfway through the roughness elements. (a) Dashed and solid lines, Stokes solution in response to a homogeneous shear; coloured background, \bar{v}_R from DNS for $k^+ \approx 6$. (b) and (c), dashed and solid lines, laminar solution in response to a homogeneous shear matching k^+ ; coloured background, \bar{v}_R from DNS for $k^+ \approx 9$ and 18, respectively.

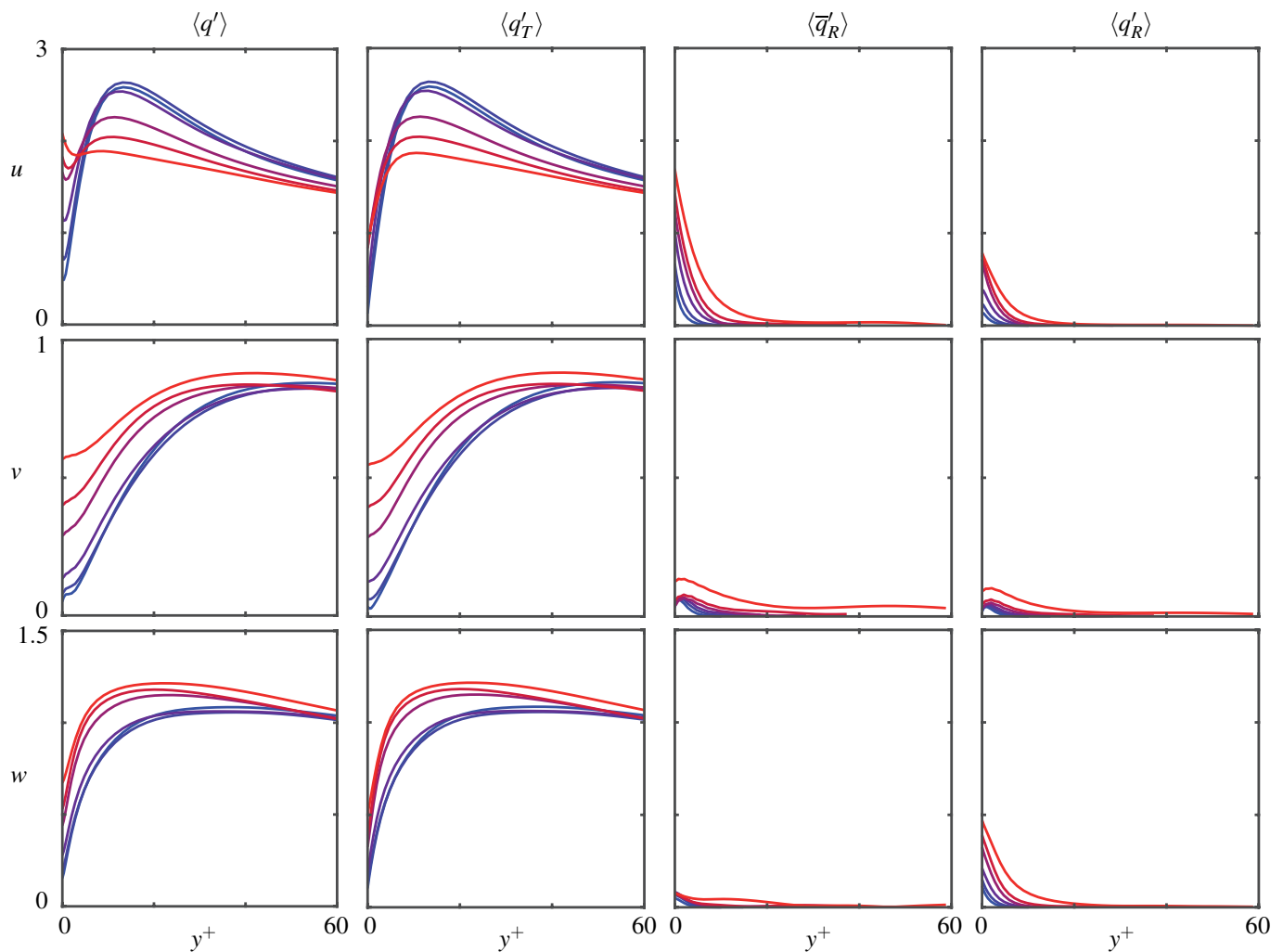


Figure 6. Root mean square of the different contributions to the streamwise velocity. From left to right, full u -signal, background-turbulence velocity u_T and roughness-induced velocity u_R . Blue to red, cases 6C through 36C. Blue to red cases 6C through 36C.

for $k^+ > 15$, or its equivalent roughness function $\Delta U^+ > 3$. This implies that the onset of roughness effects, that is, the beginning of the transitionally rough regime, can occur for roughness sizes at which the buffer-layer turbulence is essentially unaffected, so that it may be possible to estimate the changes in the flow independently of the

turbulence. It also shows that the phase-average and the modulated roughness-induced contributions are of the same order of magnitude and comparable to the turbulent contribution near the wall. Neither contribution should therefore be neglected when estimating the total fluctuations.

CONCLUSIONS AND FUTURE WORK

We have focussed the present work in the transitionally rough regime of turbulent flows over rough walls. As a starting benchmark case, we have selected a surface made up of evenly spaced, uniform cubes, and we have conducted a series of DNSs in which we have varied the size of the cubes, k^+ , while maintaining the surface shape, so that the whole transitionally rough regime could be studied. We have hypothesised that the fluctuating flow could be decomposed into a smooth-wall-like turbulent contribution and a roughness-induced one. We have checked this assumption for the fluctuating velocities. For the smaller values of k^+ , the decomposition is valid, except that the roughness-induced component is modulated in amplitude by the turbulent one. For somewhat larger k^+ , the turbulent component differs from that over smooth walls, but in the onset of the transitionally rough regime the turbulent component remains essentially smooth-like, and all the changes in the flow can then be attributed to the geometry-induced component. This result suggests that it may be possible to predict the onset of roughness effects without considering the interaction of the roughness geometry with the turbulence, but further studies are required to verify this.

This work was supported by the European Research Council through the II Multiflow Summer Workshop, and by the British Engineering and Physical Sciences Research Council through grant number EP/M506485/1.

REFERENCES

- Abderrahaman-Elena, N. & García-Mayoral, R. 2016 Geometry-induced fluctuations in the transitionally rough regime. *J. Phys. Conf. Ser.* **708**.
- Choi, H., Moin, P. & Kim, J. 1993 Direct numerical simulation of turbulent flow over riblets. *J. Fluid Mech.* **255**, 503–539.
- Chung, D., Chan, L., MacDonald, M., Hutchins, N. & Ooi, A. 2015 A fast direct numerical simulation method for characterising hydraulic roughness. *J. Fluid Mech.* **773**, 418–431.
- Colebrook, C. F. 1939 Turbulent flow in pipes, with particular reference to the transitional region between smooth and rough wall laws. *J. Inst. Civ. Eng.* **11**, 133–156.
- Colebrook, C. F. & White, C. M. 1937 Experiments with Fluid Friction in Roughened Pipes. *Proc. R. Soc. A Math. Phys. Eng. Sci.* **161** (906), 367–381.
- Darcy, H. 1857 *Recherches expérimentales relatives au mouvement de l'eau*. Paris: Mallet-Bachelier.
- Flack, K. A. & Schultz, M. P. 2010 Review of Hydraulic Roughness Scales in the Fully Rough Regime. *J. Fluids Eng.* **132**, 041203.
- Flack, K. A. & Schultz, M. P. 2014 Roughness effects on wall-bounded turbulent flows. *Phys. Fluids* **26**, 101305.
- Flack, K. A., Schultz, M. P. & Rose, W. B. 2012 The onset of roughness effects in the transitionally rough regime. *Int. J. Heat Fluid Flow* **35**, 160–167.
- Flores, Oscar & Jiménez, Javier 2010 Hierarchy of minimal flow units in the logarithmic layer. *Phys. Fluids* **22**, 1–4.
- García-Mayoral, R. & Jiménez, J. 2011a Drag reduction by riblets. *Phil. Trans. R. Soc. A* **369**, 1412–1427.
- García-Mayoral, R. & Jiménez, J. 2011b Hydrodynamic stability and breakdown of the viscous regime over riblets. *J. Fluid Mech.* **678**, 317–347.
- Hama, F. R. 1954 *Boundary-layer characteristics for smooth and rough surfaces*. New York: Society of Naval Architects and Marine Engineers.
- Jelly, T. O., Jung, S. Y. & Zaki, T. A. 2014 Turbulence and skin friction modification in channel flow with streamwise-aligned superhydrophobic surface texture. *Phys. Fluids* **26**, 095102.
- Jiménez, J. 2004 Turbulent Flows Over Rough Walls. *Annu. Rev. Fluid Mech.* **36** (1991), 173–196.
- Jiménez, J. & Moin, P. 1991 The minimal flow unit in near-wall turbulence. *J. Fluid Mech.* **225**, 213–240.
- Jiménez, J., Uhlmann, M., Pinelli, A. & Kawahara, G. 2001 Turbulent shear flow over active and passive porous surfaces. *J. Fluid Mech.* **442**, 89–117.
- Kim, H. T., Kline, S. J. & Reynolds, W. C. 1971 The production of turbulence near a smooth wall in a turbulent boundary layer. *J. Fluid Mech.* **50**, 133–160.
- Kim, J., Moin, P. & Moser, R. D. 1987 Turbulence statistics in fully developed channel flow at low Reynolds number. *J. Fluid Mech.* **177**, 133–166.
- Leonardi, S. & Castro, I. P. 2010 Channel flow over large cube roughness: a direct numerical simulation study. *J. Fluid Mech.* **651**, 519.
- Leonardi, S., Orlandi, P. & Antonia, R. A. 2007 Properties of d- and k-type roughness in a turbulent channel flow. *Phys. Fluids* **12** (19), 125101.
- Ligrani, P. M. & Moffat, R. J. 1986 Structure of transitionally rough and fully rough turbulent boundary layers. *J. Fluid Mech.* **162**, 69–98.
- Luchini, P., Manzo, F. & Pozzi, A. 1991 Resistance of a grooved surface to parallel flow and cross-flow. *J. Fluid Mech.* **228**, 87–109.
- Mathis, R., Hutchins, N. & Marusic, I. 2009 Large-scale amplitude modulation of the small-scale structures in turbulent boundary layers. *J. Fluid Mech.* **628**, 311–337.
- Nikuradse, J. 1933 Laws of flow in rough pipes. *Tech. Rep.*. NACA, Washington.
- Raupach, M. R., Antonia, R. A. & Rajagopalan, S. S. 1991 Rough-Wall Turbulent Boundary Layers. *Appl. Mech. Rev.* **44**, 1–25.
- Reynolds, W. C. & Hussain, A. K. M. F. 1972 The mechanics of an organized wave in turbulent shear flow. Part 3. Theoretical models and comparisons with experiments. *J. Fluid Mech.* **54**, 263–288.
- Schlichting, H. 1936 Experimental investigation of the problem of surface roughness. *Tech. Rep.*.
- Schultz, M. P. & Flack, K. A. 2007 The rough-wall turbulent boundary layer from the hydraulically smooth to the fully rough regime. *J. Fluid Mech.* **580**, 381.
- Seo, J., García-Mayoral, R. & Mani, A. 2015 Pressure fluctuations in turbulent flows over superhydrophobic surfaces. *J. Fluid Mech.* **783**, 448–473.
- Smith, C.R. & Metzler, S.P. 1983 Characterization of low-speed streaks in the near-wall region of a turbulent boundary layer. *J. Fluid Mech.* **129**, 27–54.
- Talluru, K. M., Baidya, R., Hutchins, N. & Marusic, Ivan 2014 Amplitude modulation of all three velocity components in turbulent boundary layers. *J. Fluid Mech.* **746**.
- Zhang, C. & Chernyshenko, S. I. 2016 Quasisteady quasihomogeneous description of the scale interactions in near-wall turbulence. *Phys. Rev. Fluids* **1** (1), 014401.